

The free surface effect on a chemotaxis–diffusion–convection coupling system

Filip Ivančić^{a,d}, Tony W.H. Sheu^{a,b,c,*}, Maxim Solovchuk^{a,d,**}

^a Department of Engineering Science and Ocean Engineering, National Taiwan University, Taipei, Taiwan

^b Center for Advanced Study in Theoretical Sciences (CASTS), National Taiwan University, Taipei, Taiwan

^c Institute of Applied Mathematical Sciences, National Taiwan University, Taipei, Taiwan

^d National Health Research Institutes, Institute of Biomedical Engineering and Nanomedicine, Zhunan, Taiwan

Received 11 February 2019; received in revised form 18 July 2019; accepted 18 July 2019

Available online 29 July 2019

Highlights

- Free surface influences the time scale on which bioconvection patterns occur.
- Convection patterns resemble to those characteristic for Bénard type convection.
- Three-dimensional results show an excellent resemblance to real experiment.

Abstract

Suspension of an oxytactic bacteria (e.g. the species *Bacillus subtilis*) placed in a container with its upper surface open to the atmosphere results in the formation of complex bioconvection patterns. The bacteria consume the oxygen diluted in the water, thereby causing the decrease of oxygen concentration everywhere except on the free surface. Through the free surface, which is in direct contact with the air, oxygen diffuses into the water. Slightly denser than water, the oxytactic bacteria are able to swim towards the higher concentration of oxygen (i.e. upwards) and they concentrate in a thin layer below the free surface. This causes the change of the suspension density and Rayleigh–Taylor type instabilities to occur. The chemotaxis phenomenon has been successfully modeled within continuum mechanics approach under certain simplifications. The set of (non-linearly) coupled equations describing the process involves the Boussinesq approximation of the Navier–Stokes equations governing the fluid motion and two convection–diffusion type equations governing the bacteria and oxygen concentrations. One of the simplifications that might significantly influence numerical simulations is the boundary condition for fluid equation on the free surface. This condition ensures that the vertical component of the velocity is zero, thus keeping the position of free surface fixed. This assumption significantly simplifies numerical procedure since the non-linearly coupled system can then be solved on stationary grid. However, allowing the motion of the free surface and completing the system with appropriate boundary conditions on contact line (liquid–solid–gas interface), a more realistic model is derived and new insights on nonlinear dynamics of the chemotaxis phenomenon are obtained. Our aims in this paper are to upgrade the currently available model into a more

* Corresponding author at: Department of Engineering Science and Ocean Engineering, National Taiwan University, Taipei, Taiwan.

** Corresponding author at: National Health Research Institutes, Institute of Biomedical Engineering and Nanomedicine, Zhunan, Taiwan.
E-mail addresses: ivancifi@gmail.com (F. Ivančić), twhsheu@ntu.edu.tw (T.W.H. Sheu), solovchuk@gmail.com (M. Solovchuk).

realistic one in both two and three dimensions, to propose a numerical procedure to deal with the new system (now posed on time-dependent domain) and, finally, to show the difference between this new model and the previous simplified one.

© 2019 Elsevier B.V. All rights reserved.

Keywords: Chemotaxis–convection–diffusion; Bioconvection; Time-dependent domain; Arbitrary Lagrangian–Eulerian framework; Surface tension; Dynamic contact line

0. Introduction

A *taxis* refers to the movement of organisms or cells in response to some (outside) stimulus whose nature can be of, for example, chemical (chemotaxis), mechanical (gyro–, hpto–, rheotaxis), physical (photo–, thermotaxis) origins. When a suspension of oxytactic bacteria in water is placed in a container with its upper surface open to the atmosphere, complex bioconvection¹ patterns occur. For bacteria of species *Bacillus subtilis*, this was experimentally observed and reported in [1] and extended in [2,3]. The bacteria consume the oxygen diluted in water causing the oxygen concentration to decrease everywhere except on the free surface. The free surface is in contact with the air so oxygen diffuses through it into the suspension. Slightly denser than water, the oxytactic bacteria are able to swim towards the higher oxygen concentration, i.e. upwards (towards the free surface), causing a nonuniform density of suspension in a sense that bacteria are concentrated in a thin layer below the free surface. When vertical density gradient becomes large enough, an overturning (Rayleigh–Taylor like) instability occurs.

The set of (non-linearly) coupled equations governing the phenomenon involves Navier–Stokes equations describing the fluid motion and two convection–diffusion type equations describing the oxygen and bacteria concentrations (the Keller–Segel equations). In [2,3] a theoretical insight for modeling the phenomenon within the continuum mechanics approach is given, numerical simulations for both shallow and deep layer containers were performed and the linear instability analysis for the steady-state cell and oxygen concentration distributions were carried out. In [4] a high-resolution vorticity-based hybrid finite-volume finite-difference scheme was derived with which they investigated the nonlinear dynamics of a two dimensional chemotaxis–diffusion–convection system. In [5] an upwind finite element method was developed in order to investigate the pattern formation and hydrodynamical stability of the system.

One of the simplifications that might significantly influence the numerical results, and which was made in all of the previously mentioned works, is a condition on the free surface that keeps it stationary during the simulation. This condition is manifested through Dirichlet boundary conditions in the Navier–Stokes equations prescribing the vertical component of the velocity to be zero and, consequently, disabling the motion of the free surface. This assumption significantly simplifies the numerical procedure since the non-linearly coupled system is then solved on a stationary grid. However, allowing the motion of the free surface and completing the system with appropriate boundary conditions on the contact line (liquid–solid–gas interface), a much more realistic model is obtained and new insights on nonlinear dynamics of the chemotaxis phenomenon might be drawn. In [6], a two dimensional chemotaxis–diffusion–convection coupling system with deformed free surface has been considered and the influence of aggregation of oxytactic cells on the deformed free surface of a shallow container has been studied analytically.

The aim of this paper is three-fold: to upgrade the currently available model into the more realistic one in both two and three dimensions, to propose a numerical procedure to deal with the new system (now posed on time-dependent domain), and, finally, to show that influence of the free surface matters. The numerical method of choice in this paper will be the *finite element method* (FEM) within *Arbitrary Lagrangian–Eulerian* (ALE) framework [7–9] – a natural choice for the problem described above. The model will be upgraded in the rest of the paper in the sense that dynamic free surface will be considered. The only difference between the new and previous models will be in the boundary conditions of Navier–Stokes equations. Allowing the free surface to move raises a few additional questions, both from modeling and purely numerical points of views. From the modeling point of view, specification of boundary conditions on fluid–solid–gas interface (the contact line in three dimensions and contact points in two dimensions) presents a major issue. Classically used, the so-called, *no-slip* boundary conditions and experimentally observed moving contact line (points) result in contradictory demands. The so-called *generalized*

¹ Bioconvection is a general term describing the phenomenon in fluid dynamics which is driven by collective swimming motion of the large number of small organisms (such as bacteria or algae) in the fluid.

Navier boundary condition (GNBC) extended from molecular dynamics approach to continuum mechanics model introduced in [10,11] deals with this manner. Another issue arising from the dynamic free surface is the appearance of the surface tension – a stress which arises on fluid–fluid interface in case of two immiscible fluids. Surface tension is balanced by pressure and curvature via the Young–Laplace equation. As soon as the surface is not flat any longer, the curvature is non-zero. Since surface tension is, roughly speaking, the tendency of fluid surface to shrink into the minimum surface area, it might play a significant role in overall phenomenon. However, from the numerical point of view curvature is very hard and tricky to handle since approximation of the domain boundary is by piecewise linear segments in two dimensions and triangles in three dimensions. A particularly elegant solution to this problem lies in the *Laplace–Beltrami operator* which allows to express the curvature in the weak form and is, therefore, easily adapted to finite element method (see [12,13] and references therein).

There are two important issues from numerical perspective specific for finite element method within ALE framework and they manifest themselves in the form of artificial sinks and/or sources. One of the issues deals with the determination of the domain boundary displacement in a way that the total volume of the fluid is preserved — an obvious requirement for problems involving incompressible fluids yet very non-trivial on the discrete level. Another issue deals with integrating the equations in time and is called the *Space conservation law* (SCL) (see [14,15]). The SCL problematics is characteristic for conservative form of equations written in ALE frame — conservative in a sense that the transient term is expressed as a total time derivative (we discuss this manner later in more details).

The paper is organized as follows: In Section 1, we recall the existing simplified model for chemotaxis–diffusion–convection (CDC) coupling system. In Section 2, we propose a generalization of CDC model which includes the dynamic free surface and appropriate boundary conditions. In Section 3, we propose a numerical procedure to solve the CDC system on time dependent grid. In Section 4, we present the numerical results and emphasize the influence of the free surface to the overall phenomenon. Finally, in Section 5, we summarize what have been done and draw the conclusions.

1. Chemotaxis–diffusion–convection (CDC) coupling system

In this section we recall and summarize the system of equations governing the chemotaxis–convection–diffusion phenomenon under the assumption that motion of free surface is negligible. This system was already analyzed and discussed in [2–5] where the non-dimensionalization was proposed in order to make it feasible for the numerical implementation as well as for the parametric studies.

1.1. The dimensional CDC system

The domain occupied by the suspension of bacteria (in water) at time $t \in [0, T]$ is denoted by $\Omega(t)$, where $[0, T]$ is the time interval during which we consider the phenomenon under investigation. It is assumed that domain width is much larger than its height. The ratio between the domain height and width is denoted by ε and we are typically interested in cases for $\varepsilon \ll 1$. The boundary $\partial\Omega$ consists of the fixed rigid walls Γ and fixed free surface Σ :

$$\partial\Omega = \Gamma \cup \Sigma.$$

The set of contact points in two dimensional case or contact line in three dimensional case is then given as:

$$\partial\Sigma = \Gamma \cap \Sigma.$$

Due to the assumption of fixed free surface, the domain Ω is time independent during the whole process. By \mathbf{n} and \mathbf{t} we denote normal and tangent to the $\partial\Omega$, respectively. The sketch of the domain of interest is given in Fig. 1.

The CDC phenomenon within continuum mechanics environment is described by the set of equations governing the fluid motion (the Navier–Stokes equations) and the equations governing the oxygen and bacteria concentrations (two convection–diffusion equations). In what follows, \mathbf{v} denotes the fluid velocity, p the fluid pressure, c the oxygen concentration and n the bacteria concentration — these are the unknowns of the CDC system. Parameters determining the physical properties of the CDC system are the fluid density ρ_w and dynamic viscosity μ . The volume of the bacterium is denoted by V_b and the volumetric mass, which is slightly larger than the fluid density, by ρ_b . The bacterium diffusivity, D_b , comes from a random swimming of bacteria (details can be found in [2]). The oxygen diffuses into the water with its diffusivity constant, D_o , and is consumed by bacteria with the bacterial oxygen consumption rate, κ_b , that is proportional to the concentration of the cells, n . Consequently, owing to the chemotaxis

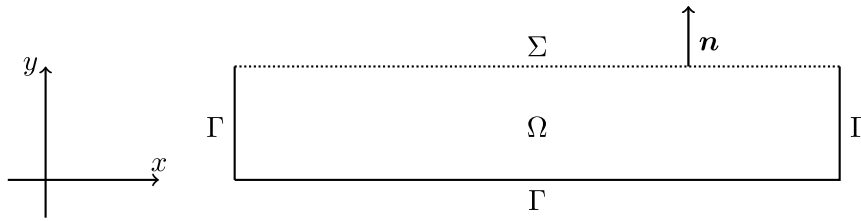


Fig. 1. The sketch of domain occupied by the suspension of bacteria in water.

Table 1
Nomenclature description.

Parameter	Definition	Dimension
\mathbf{v}	Fluid velocity	m s^{-1}
p	Fluid pressure	Pa
c	Oxygen concentration	molecules m^{-3}
n	Bacteria number density	m^{-3}
ρ_w	Fluid density	kg m^{-3}
μ	Fluid dynamic viscosity	$\text{kg m}^{-1} \text{s}^{-1}$
ρ_b	Bacteria volumetric mass density	kg m^{-3}
\mathbf{g}	Gravitational acceleration	m s^{-2}
D_b	Bacteria diffusivity	$\text{m}^2 \text{s}^{-1}$
S_b	Chemotactic sensitivity	$\text{m}^5 \text{s}^{-1}$
D_O	Oxygen diffusivity	$\text{m}^2 \text{s}^{-1}$
κ_b	Oxygen consumption rate	$\text{molecules cell}^{-1} \text{s}^{-1}$
σ	Surface tension	N m^{-1}
β	Friction slip coefficient	Pa s m^{-1}

response, bacteria direct its movement towards the higher concentration of oxygen (directional swimming). Such a movement of bacteria depends on the chemotactic sensitivity, S_b . When the oxygen concentration becomes lower than some threshold values, the bacteria become inactive — they will stop both consuming oxygen and swimming towards higher concentration of it. This property is expressed by a *cut-off* function $r = r(c)$ which is modeled as a step function based on experiments [2,3]. For a summary of nomenclature, see Table 1.

The full dimensional system in $\Omega \times (0, T)$ reads:

$$\begin{aligned}
 \partial_t c + \mathbf{v} \cdot \nabla c - D_O \Delta c &= -\kappa_b r(c)n, \\
 \partial_t n + \mathbf{v} \cdot \nabla n - D_b \Delta n + \nabla \cdot [S_b r(c)n \nabla c] &= 0, \\
 \rho_w (\partial_t \mathbf{v} + \mathbf{v} \cdot \nabla \mathbf{v}) - \text{div } \boldsymbol{\sigma}_d &= n \mathbf{V}_b \Delta \rho \mathbf{g}, \\
 \text{div } \mathbf{v} &= 0,
 \end{aligned}
 \tag{1}$$

where

$$\begin{aligned}
 \boldsymbol{\sigma}_d &= -p_d \mathbb{I} + \mu \mathbb{D}(\mathbf{v}), \\
 \mathbb{D}(\mathbf{v}) &= \nabla \mathbf{v} + \nabla \mathbf{v}^T,
 \end{aligned}$$

$\mathbf{g} = [0, -g]^T$ in 2D case and $\mathbf{g} = [0, 0, -g]^T$ in 3D case with g being the gravitational acceleration and $\Delta \rho = \rho_b - \rho_w$ being the difference between bacterium and water densities. Subscript d in p_d denotes that the considered pressure is the dynamic pressure, i.e.:

$$p = p_d + \rho_w \mathbf{g} \cdot \mathbf{x}, \quad \mathbf{x} = (x, y) \text{ in } \mathbb{R}^2, \quad \mathbf{x} = (x, y, z) \text{ in } \mathbb{R}^3
 \tag{2}$$

and σ_d is the stress tensor corresponding to the dynamic pressure. The system is completed by the following boundary and initial conditions:

$$\begin{aligned}
 \mathbf{v} &= 0 \text{ on } \Gamma \text{ (no-slip boundary condition),} \\
 \mathbf{v} \cdot \mathbf{n} &= 0 \text{ on } \Sigma \text{ (zero velocity in vertical direction),} \\
 \boldsymbol{\sigma} \mathbf{n} \cdot \mathbf{t} &= 0 \text{ on } \Sigma \text{ (do-nothing boundary condition in tangential direction),} \\
 \nabla c \cdot \mathbf{n} &= 0 \text{ on } \Gamma \text{ (no-flux of oxygen through the rigid walls),} \\
 c &= c_{air} \text{ on } \Sigma \text{ (on surface oxygen diffuses freely from the air),} \\
 [\mathbf{D}_b \nabla n - S_b r(c)n \nabla c] \cdot \mathbf{n} &= 0 \text{ on } \partial \Omega \text{ (no-flux of bacteria through the boundary),} \\
 \mathbf{v}(0) &= 0 \text{ in } \Omega, \\
 c(0) &= c_0 \text{ in } \Omega, \\
 n(0) &= n_0 \text{ in } \Omega.
 \end{aligned} \tag{3}$$

Subjected to the incompressibility constraint, the fluid equations employ the Boussinesq approximation in which density variations appear only in the buoyant forcing term. Both bacteria and oxygen concentrations are advected by the fluid. Furthermore, as discussed in [3], it is assumed that the timescale for which biological growth and decay of bacteria are significant is much greater than that required for bioconvection pattern formation. Therefore, the total number of cells is assumed to be conserved during the time interval of interest.

1.2. The dimensionless CDC system

In order to perform a systematical parametric study as well as for an efficient numerical implementation, the CDC system is non-dimensionalized. The non-dimensionalization is performed as in [3–5] and by *overline* we denote the dimensionless quantities.

The characteristic length L is defined by the container height h , $L = h$, and the characteristic time is dictated by the bacteria diffusivity constant, $t_c = h^2 / D_b$. Characteristic velocity and pressure are, respectively, given by:

$$U = \frac{D_b}{L} \text{ and } p_c = \frac{\mu U}{L}. \tag{4}$$

Dimensionless variables are then defined as follows:

$$\begin{aligned}
 \bar{\mathbf{x}} &= \frac{\mathbf{x}}{h}, \bar{t} = \frac{t}{h^2 / D_b}, \\
 \bar{c} &= \frac{c}{c_{air}}, \bar{n} = \frac{n}{n_0}, \bar{\mathbf{v}} = \frac{\mathbf{v}}{D_b / h}, \bar{p} = \frac{p}{\mu D_b / h^2},
 \end{aligned} \tag{5}$$

where

$$\bar{n}_0 = \frac{1}{|\Omega|} \int_{\Omega} n_0 d\mathbf{x}$$

is the average concentration of the initial bacterial population. The CDC system is characterized by the five dimensionless parameters given by

$$\begin{aligned}
 \text{Pr} &= \frac{\mu}{\rho_w D_b}, \text{Ra} = \frac{h^3}{D_b \mu} g V_b \bar{n}_0 \Delta \rho, \\
 \text{S} &= \frac{S_b c_{air}}{D_b}, \text{H} = \frac{\kappa_b \bar{n}_0 h^2}{D_b c_{air}}, \text{Le} = \frac{D_O}{D_b},
 \end{aligned} \tag{6}$$

where Pr is the taxis Prandtl number, Ra the taxis Rayleigh number, and Le the taxis Lewis number. These numbers are analogous to the respective quantities in mass and heat transfer. S is the dimensionless chemotaxis sensitivity and H is the chemotaxis head — they characterize the chemotaxis system. The threshold value of c for the *cut-off* function r is $c^* = 0.3$ in the dimensionless environment as discussed in [4,5].

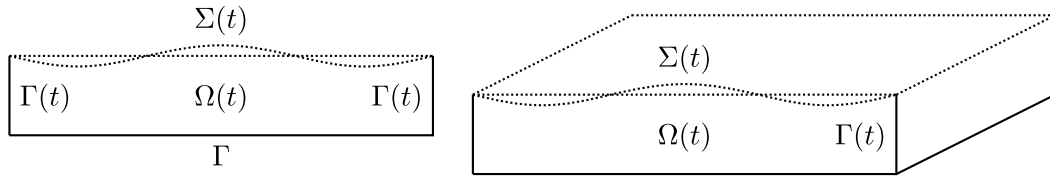


Fig. 2. The sketch of domain with the dynamic free surface.

Employing the dimensionless quantities but dropping the *overline* in order to simplify the notation (since we will only deal with the dimensionless system from now on), the scaled domain reads:

$$\Omega = [-l, l] \times [0, 1], \forall t \in [0, T], \text{ where } l \text{ is s.t. } \varepsilon = \frac{1}{2l}.$$

The dimensionless system now reads:

$$\begin{aligned} \partial_t c + \mathbf{v} \cdot \nabla c - \text{Le} \Delta c &= -\text{Hr}(c)n, \\ \partial_t n + \mathbf{v} \cdot \nabla n - \Delta n + \text{div}[\text{Sr}(c)n \nabla c] &= 0, \\ \partial_t \mathbf{v} + \mathbf{v} \cdot \nabla \mathbf{v} - \text{Pr} \text{div} \boldsymbol{\sigma} &= -\text{Ra} \text{Pr} \mathbf{k}, \\ \text{div} \mathbf{v} &= 0, \end{aligned} \tag{7}$$

in $\Omega \times (0, T)$ where $\mathbf{k} = [0, 1]^T$. The Neumann type boundary conditions remain the same as those in the dimensional case, while the Dirichlet type boundary conditions have to be non-dimensionalized accordingly:

$$\begin{aligned} \mathbf{v} &= 0 \text{ on } \Gamma \text{ (no-slip boundary condition),} \\ \mathbf{v} \cdot \mathbf{n} &= 0 \text{ on } \Sigma \text{ (zero velocity in vertical direction),} \\ \boldsymbol{\sigma} \mathbf{n} \cdot \mathbf{t} &= 0 \text{ on } \Sigma \text{ (do-nothing boundary condition in tangential direction),} \\ \nabla c \cdot \mathbf{n} &= 0 \text{ on } \Gamma \text{ (no-flux of oxygen through the rigid walls),} \\ c &= 1 \text{ on } \Sigma \text{ (on surface, oxygen diffuses freely from the air),} \\ [-\nabla n + \text{Sr}(c)n \nabla c] \cdot \mathbf{n} &= 0 \text{ on } \partial \Omega \text{ (no-flux of bacteria through the boundary),} \\ \mathbf{v}(0) &= 0 \text{ in } \Omega, \\ c(0) &= c_0/c_{air} \text{ in } \Omega, \\ n(0) &= n_0/\bar{n}_0 \text{ in } \Omega. \end{aligned} \tag{8}$$

2. Augmented CDC system with time-dependent free surface

In order to allow free surface to move and deform, i.e. considering a dynamic free surface, the boundary conditions in the Navier–Stokes equation have to be changed. Once the free surface Σ is disturbed, its curvature becomes non-trivial and surface tension effect appears. The disturbance of the Σ is expected to be very small and, consequently, the surface tension effects are not expected to play major role far from the rigid walls. Near the rigid walls, due to the tendency of fluid velocity to be equal to the wall velocity (classically incorporated in the *no-slip* boundary conditions), and pressure jump across the free surface, surface tension influences the geometry of the free surface (capillary effects). From physical observations, it is known that *no-slip* boundary conditions very well describe the behavior of the fluid in contact with the rigid walls, but, at the same time, the contact line (interface between solid, liquid and gaseous phases) can move. Within continuum mechanics approach these are two contradictory conditions on the same part of the boundary. As a result, they indeed demand an additional attention.

In Fig. 2, a sketch of the domain with the dynamic free surface is shown in two and three dimensions. Note that in the case we are considering now, the free surface and the fluid elevation on walls may vary with time, while the bottom is fixed.

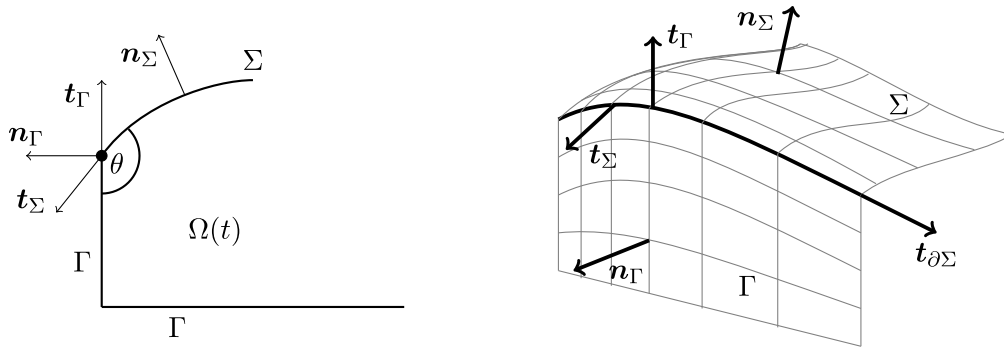


Fig. 3. The sketch of part of the domain near the contact line with the various unit vectors necessary for formulating the boundary conditions.

2.1. The generalized Navier boundary conditions

Recall that the *no-slip* boundary condition is just an approximation of the more general *Navier-slip* boundary condition:

$$\beta(\mathbf{v} - \mathbf{w}) \cdot \boldsymbol{\tau} + \boldsymbol{\sigma} \mathbf{n} \cdot \boldsymbol{\tau} = 0 \text{ on } \Gamma, \forall \boldsymbol{\tau} \text{ tangent to } \Gamma,$$

where β is the friction slip coefficient and \mathbf{w} is the boundary velocity (in all our cases $\mathbf{w} = 0$). In practice, the coefficient β is very large justifying the application of the *no-slip* approximation

$$\beta(\mathbf{v} - \mathbf{w}) \cdot \boldsymbol{\tau} = 0 \text{ on } \Gamma, \forall \boldsymbol{\tau} \text{ tangent to } \Gamma.$$

As already mentioned, the *Navier-slip* boundary condition fails to adequately describe the behavior of the dynamic contact line. For that reason, the *generalized Navier boundary condition (GNBC)* extended from the molecular dynamics approach to the continuum mechanics approach was introduced in [10,11]. To state them, the following vectors and orientations have to be defined (see Fig. 3). Denote by \mathbf{n}_Σ and \mathbf{n}_Γ the unit normal vectors to the free surface and the rigid walls, respectively. Then, on the boundary of the free surface $\partial\Sigma$, we define the tangent vector to $\partial\Sigma$ by $\mathbf{t}_{\partial\Sigma} = \mathbf{n}_\Sigma \times \mathbf{n}_\Gamma$, the tangent vector to Σ (lies in tangential plane of Σ) by $\mathbf{t}_\Sigma = \mathbf{t}_{\partial\Sigma} \times \mathbf{n}_\Sigma$, and the tangent vector to the wall Γ perpendicular to the $\partial\Sigma$ by $\mathbf{t}_\Gamma = \mathbf{n}_\Gamma \times \mathbf{t}_{\partial\Sigma}$. Note that $(\mathbf{t}_{\partial\Sigma}, \mathbf{n}_\Sigma, \mathbf{t}_\Sigma)$ and $(\mathbf{t}_{\partial\Sigma}, \mathbf{t}_\Gamma, \mathbf{n}_\Gamma)$ form positively oriented orthonormal basis.

Now it is possible to define a dynamic contact angle – an angle that is formed between the free surface and rigid wall – by:

$$\cos \theta = \mathbf{t}_\Sigma \cdot \mathbf{t}_\Gamma. \tag{9}$$

In addition, a *static contact angle* θ_s has to be provided as an input parameter (an *a priori* known value). When fluid is at rest i.e. all forces acting on it are in balance, the dynamic contact angle equals to the static one. We refer to [10,11] for details on this manner. We mention that the estimation of θ_s is a hard problem from both theoretical and experimental standpoints and its value depends on the natures of fluid and contact wall. The essential idea behind the GNBC is as follows: they are obtained by breaking the Cauchy stress vector into its normal and tangential parts. Stress on the contact line is then introduced into the equation using the (surface) Greens formula (for more details on this manner one can also check Section 3.1). Let \mathbf{n} and $\boldsymbol{\tau}$ be the normal and tangential vectors to the $\partial\Omega$, and assume that $\partial\Omega$ and $\partial\Sigma$ are sufficiently smooth so that all calculations below make sense. Then, assuming there is *no-flux* of fluid through the rigid wall, $\mathbf{v} \cdot \mathbf{n} = 0$ on Γ , the stress on the boundary $\partial\Omega$ can be decomposed as follows

$$\begin{aligned} - \int_{\partial\Omega} \boldsymbol{\sigma} \mathbf{n} \, dS &= - \int_{\partial\Omega} ((\boldsymbol{\sigma} \mathbf{n} \cdot \mathbf{n})\mathbf{n} + (\boldsymbol{\sigma} \mathbf{n} \cdot \boldsymbol{\tau})\boldsymbol{\tau}) \, dS \\ &= \int_\Gamma (\beta \mathbf{v} \cdot \boldsymbol{\tau})\boldsymbol{\tau} \, dS + \int_{\partial\Sigma} (\sigma(\mathbf{t}_\Sigma \cdot \mathbf{t}_\Gamma - \cos \theta_s)\mathbf{t}_\Gamma \cdot \boldsymbol{\tau})\boldsymbol{\tau} \, ds - \int_\Sigma \boldsymbol{\sigma} \mathbf{n} \, dS, \end{aligned} \tag{10}$$

where σ is the surface tension. Eq. (10) simply decomposes stress on the boundary into sum of the stress on each particular component of the boundary. For detailed derivation we refer to [10,11]. The first term comes from

the Navier–slip boundary condition while the second term is the novelty introduced to deal with dynamic contact line. The third term has to compensate for the pressure jump in the normal direction which is expressed through surface tension and surface curvature, and for the stress in tangential direction which is non-zero if surface tension is non-constant. In [11], authors refer to the $(\mathbf{t}_\Sigma \cdot \mathbf{t}_\Gamma - \cos \theta_s)$ as *uncompensated Young stress*. Essentially, it measures the force on the contact line when dynamic contact angle differs from the static one. Thus, in compact notation, the GNBC can be written in the form of:

$$\beta(\mathbf{v} - \mathbf{w}) \cdot \boldsymbol{\tau} + \boldsymbol{\sigma} \mathbf{n} \cdot \boldsymbol{\tau} + \sigma(\mathbf{t}_\Sigma \cdot \mathbf{t}_\Gamma - \cos \theta_s) \mathbf{t}_\Gamma \cdot \boldsymbol{\tau} \delta_{\partial \Sigma} = 0 \text{ on } \Gamma, \forall \boldsymbol{\tau} \text{ tangent to } \Gamma, \tag{11}$$

where $\delta_{\partial \Sigma}$ is the distribution which localizes the last term to the $\partial \Sigma \subset \Gamma$.

2.2. Augmented CDC system with dynamic free surface

Finally, we are able to extend the CDC system from the literature into the fully realistic one for handling the dynamic contact line by employing the GNBC. We use the same scaling process as that described in the previous section for the simplified model. However, three new dimensionless numbers characterizing the system come into play from surface tension and friction slip coefficients contribution, and from the change of the hydrodynamic part of the pressure due to surface distortion: the capillary number Ca , dimensionless friction slip parameter β_s and the Froude number Fr

$$Ca = \frac{D_b \mu}{\sigma_0 h}, \beta_s = \frac{\rho_w D_b h}{\beta}, Fr = \frac{U^2}{gL}, \tag{12}$$

where σ_0 is the characteristic surface tension (see Remark 2.1). The dimensionless surface tension is introduced naturally as

$$\bar{\sigma} = \frac{\sigma}{\sigma_0}. \tag{13}$$

Remark 2.1. It has to be mentioned that the surface tension σ is not constant in reality. It is a function of bacteria concentration n , $\sigma = \sigma(n)$, and, generally, higher concentrations of bacteria on surface Σ decrease the surface tension of the fluid. Reasons for that have not been well investigated. There are some indications that physical presence of bacterial cells itself plays an important role in this connection. Furthermore, some bacteria are known to produce surface-active chemical components which influence the surface tension. Inclusion of this into the CDC system would result in some convection–diffusion type surface PDE governing the law for surface tension of the suspension. Keeping in mind phenomenon of flows in thin liquid films arising due to thermal gradients, one may predict what types of instabilities are to be expected. Aside from already mentioned Bénard–Taylor type instabilities, Marangoni–Benard convection effect appears by including the dependence of surface tension on the temperature [16]. Similar behavior is most likely to be expected by including the dependence of surface tension on bacteria concentration. This, however, outreaches the scope of this paper. Some information on the influence of surfactants onto the surface tension can be found in [17]. Although a fully general model considering σ to be a function of bacteria concentration n is developed, for the numerical simulations in this paper σ is taken to be constant independently on the bacteria concentration, $\sigma = \sigma_0$. A more complicated situation may be studied in the future. σ_0 denotes the surface tension characteristic for the fluid without the presence of bacteria.

Remark 2.2. One should also notice that the characteristic length is taken to be a height of the container h . While this selection for the characteristic length makes sense for the other nondimensional numbers, for the capillary number one should proceed carefully. Strictly speaking, the characteristic length in any dimensionless number related to the surface tension effects should be somehow related to the radius of the curvature [18], which is very different from the container height (significantly larger). However, the chemotaxis phenomenon is greatly determined by depth of the container (shallow versus deep container) and most reasonable characteristic length should be chosen as the container depth. Although this selection for the characteristic length gives a distorted intuition on capillary number, the compensation for surface tension effect comes through the free surface curvature term (see the dimensionless governing equations).

The only difference introduced in the model is the boundary conditions in Boussinesq approximation of the Navier–Stokes equations. The full system now reads:

$$\begin{aligned}
 \partial_t c + \mathbf{v} \cdot \nabla c - \text{Le} \Delta c &= -\text{Hr}(c)\mathbf{n}, \\
 \partial_t \mathbf{n} + \mathbf{v} \cdot \nabla \mathbf{n} - \Delta \mathbf{n} + \text{div}[\text{Sr}(c)\mathbf{n}\nabla c] &= 0, \\
 \partial_t \mathbf{v} + \mathbf{v} \cdot \nabla \mathbf{v} - \text{Pr} \text{div} \boldsymbol{\sigma} &= -\text{Fr}^{-1} \mathbf{k} - \text{Ra} \text{Pr} n \mathbf{k}, \\
 \text{div} \mathbf{v} &= 0,
 \end{aligned}
 \tag{14}$$

in $\bigcup_{t \in (0, T)} \Omega(t) \times \{t\}$, which in the rest of the paper we compactly denote by $\Omega(t) \times (0, T)$. Note that now the domain Ω is function of time, $\Omega = \Omega(t)$. The pressure considered now is the total pressure rather than the dynamic one in order to simplify the boundary conditions, and consequently introducing an extra term in the Navier–Stokes equations, the term $-\text{Fr}^{-1} \mathbf{k}$. It is possible to scale the equations with respect to the dynamic pressure as in previous case, but then an extra term in the boundary conditions will appear to compensate for the hydrodynamic pressure change due to the surface distortion. The boundary and initial conditions completing the system are as follows ($\boldsymbol{\tau}$ is an arbitrary tangent vector and \mathbf{n} is an outer unit normal vector to the $\partial\Omega$)

$$\begin{aligned}
 \text{Pr} \boldsymbol{\sigma} \mathbf{n}_\Gamma \cdot \boldsymbol{\tau} &= -\beta_s^{-1}(\mathbf{v} - \mathbf{w}) \cdot \boldsymbol{\tau} - \text{Pr} \text{Ca}^{-1}(\mathbf{t}_\Sigma \cdot \mathbf{t}_\Gamma - \cos \theta_s) \mathbf{t}_\Gamma \cdot \boldsymbol{\tau} \delta_{\partial\Sigma} \text{ on } \Gamma, \forall \boldsymbol{\tau}, \\
 \mathbf{v} \cdot \mathbf{n}_\Gamma &= 0 \text{ on } \Gamma, \\
 \boldsymbol{\sigma} \mathbf{n}_\Sigma \cdot \boldsymbol{\tau} &= -\text{Pr} \text{Ca}^{-1} \nabla_\Sigma \boldsymbol{\sigma} \cdot \boldsymbol{\tau} \text{ on } \Sigma, \forall \boldsymbol{\tau}, \\
 \text{Pr} \boldsymbol{\sigma} \mathbf{n}_\Sigma \cdot \mathbf{n}_\Sigma &= \text{Pr} \text{Ca}^{-1} \sigma \kappa \text{ on } \Sigma, \\
 \nabla c \cdot \mathbf{n}_\Gamma &= 0 \text{ on } \Gamma, \\
 c &= 1 \text{ on } \Sigma, \\
 \nabla n \cdot \mathbf{n} &= 0 \text{ on } \partial\Omega, \\
 \mathbf{v}(0) &= 0 \text{ in } \Omega(0), \\
 c(0) &= c_0/c_{air} \text{ in } \Omega(0), \\
 n(0) &= n_0/\bar{n}_0 \text{ in } \Omega(0), \\
 \Omega(0) &= \Omega(0).
 \end{aligned}
 \tag{15}$$

Above, ∇_Σ denotes the surface gradient and κ the surface curvature (see Section 3.1).

One should note the additional non-linearity in problem formulation: the unknowns (\mathbf{v}, p, c, n) are all functions of time which are at a time $t \in [0, T]$ defined on $\Omega(t)$. However, at time $t \in (0, T]$ domain $\Omega(t)$ is itself unknown and is an implicit function of \mathbf{v} . This issue presents a serious problem from the numerical point of view and is hard to handle. We discuss it in more details in the following section.

3. Numerical procedure with finite element method

The finite element method is based on the weak form of the problem of interest. Therefore, we have to reformulate the CDC system into its weak form. The equations are first multiplied by the so-called test functions from the appropriate function spaces. Then, by means of partial integration the order of the equations is lowered employing the boundary conditions in the process [7,9].

The following test function spaces are needed in order to obtain the weak formulation: for $\Omega \subseteq \mathbb{R}^d$ with Lipschitz continuous boundary

$$\begin{aligned}
 \text{H}_{n, \Gamma}^1(\Omega; \mathbb{R}^d) &= \{\boldsymbol{\phi} \in \text{H}^1(\Omega; \mathbb{R}^d) \mid \boldsymbol{\phi} \cdot \mathbf{n}_\Gamma = 0 \text{ on } \Gamma\}, \\
 \text{L}_0^2(\Omega) &= \{q \in \text{L}^2(\Omega) \mid \int_\Omega p \, dx = 0\}, \\
 \text{H}_\Sigma^1(\Omega) &= \{\psi \in \text{H}^1(\Omega) \mid \boldsymbol{\phi} = 0 \text{ on } \Sigma\},
 \end{aligned}
 \tag{16}$$

where L^2 is the standard Lebesgue space of square integrable functions and H^1 is the standard Sobolev space, where function values on the boundaries are understood in the sense of traces. More details on functional analysis for weak formulation of partial differential equations can be found in [7,8] and references therein. In the present case, however, $\Omega = \Omega(t)$ is a function of time and test function spaces have to be adapted accordingly. In ALE frame, this generalization is straightforward as we shall show later.

3.1. The curvature in weak form

Before formulating the problem in the weak form, we pay some extra attention on handling the curvature term in the Navier–Stokes equations. Employing the techniques from the field of differential geometry, $\kappa \mathbf{n}_\Sigma$ can be rewritten in a more convenient form for finite element method in the ALE frame. Denote by ∇_Σ the surface gradient which is defined by

$$\nabla_\Sigma = [\mathbb{I} - \mathbf{n}_\Sigma \otimes \mathbf{n}_\Sigma] \nabla, \tag{17}$$

$\mathbf{n}_\Sigma \otimes \mathbf{n}_\Sigma$ being the tensor product of two vectors. Classical result from differential geometry then states

$$\Delta_\Sigma \text{id} = \kappa \mathbf{n}_\Sigma, \tag{18}$$

Δ_Σ being the *Laplace–Beltrami operator* – essentially, one can think of it as of surface Laplacian – and id being the identity function, $\text{id}: \mathbf{x} \mapsto \mathbf{x}$. For the Laplace–Beltrami operator, the analogous version of Greens formula given below holds, i.e. for \mathbf{u}, \mathbf{v} smooth

$$\int_\Sigma \Delta_\Sigma \mathbf{u} \cdot \mathbf{v} \, dS = \int_{\partial\Sigma} \nabla_\Sigma \mathbf{u} \mathbf{t}_\Sigma \cdot \mathbf{v} \, ds - \int_\Sigma \nabla_\Sigma \mathbf{u} : \nabla_\Sigma \mathbf{v} \, dS. \tag{19}$$

The above identity has been proven to be exceptionally useful in treating the boundary curvature on the discrete meshes. Calculating the curvature, which traditionally involves the second order derivatives, is a problematic manner on discrete surfaces. The Laplace–Beltrami operator not only lowers the order of derivatives involved, but also naturally allows us to express the curvature in the weak form which is very natural in the context of finite elements. To be more precise, the following identity can be derived: for $\psi \in H^1_{n,\Gamma}(\Omega; \mathbb{R}^d)$

$$\begin{aligned} \int_\Sigma \kappa \mathbf{n}_\Sigma \cdot \psi \, dS &= \int_\Sigma \Delta_\Sigma \text{id} \cdot \psi \, dS = \int_{\partial\Sigma} \nabla_\Sigma \text{id} \mathbf{t}_\Sigma \cdot \psi \, ds - \int_\Sigma \nabla_\Sigma \text{id} : \nabla_\Sigma \psi \, dS \\ &= \int_{\partial\Sigma} (\mathbf{t}_\Sigma \cdot \mathbf{t}_\Gamma) \mathbf{t}_\Gamma \cdot \psi \, ds - \int_\Sigma \nabla_\Sigma \text{id} : \nabla_\Sigma \psi \, dS, \end{aligned} \tag{20}$$

where we decomposed the test function $\psi \in H^1_{n,\Gamma}(\Omega; \mathbb{R}^d)$ into its normal and tangential parts, and then employed the property of the space $H^1_{n,\Gamma}(\Omega; \mathbb{R}^d)$ that $\psi \cdot \mathbf{n}_\Gamma = 0$ on Γ ($\partial\Sigma \subset \Gamma$).

Remark 3.1. In the two dimensional case the curvature can be expressed as an *arc-length* derivative of the tangent, i.e.

$$\kappa \mathbf{n} = \frac{d\mathbf{t}}{ds},$$

resulting in an identity

$$\int_\Sigma \frac{d\mathbf{t}}{ds} \cdot \psi \, ds = \mathbf{t} \cdot \psi \Big|_{\partial\Sigma} - \int_\Sigma \mathbf{t} \cdot \nabla \psi \mathbf{t} \, ds.$$

3.2. The weak formulation of CDC system in ALE frame

In order to include the domain time-dependency into the formulation, the Arbitrary Lagrangian–Eulerian (ALE) framework is employed [9]. Let $\widehat{\Omega} \subset \mathbb{R}^d$, $d = 2, 3$, be a fixed referential domain and $\Omega(t) \equiv \Omega_t \subset \mathbb{R}^d$ the current (physical) domain occupied by the fluid. It is assumed that boundaries of the domain are sufficiently smooth – this

usually refers to the Lipschitz continuous boundary – and that the domain evolution can be followed through a one-parameter family of mappings $(\widehat{\mathcal{A}}_t)_{t \in [0, T]} \equiv (\widehat{\mathcal{A}}(\cdot, t))_{t \in [0, T]}$, $T < \infty$,

$$\begin{aligned} \widehat{\mathcal{A}}_t: \widehat{\Omega} &\rightarrow \mathbb{R}^d, t \in [0, T], \\ (\widehat{\mathbf{x}}, t) &\mapsto (\mathbf{x}, t), \widehat{\mathbf{x}} \in \widehat{\Omega}, \mathbf{x} \in \Omega(t), \end{aligned} \tag{21}$$

i.e. $\widehat{\mathcal{A}}_t$ maps the reference domain into the current (physical) domain, $\widehat{\Omega} \mapsto \Omega_t \equiv \Omega(t) = \widehat{\mathcal{A}}_t(\widehat{\Omega})$. By $\widehat{\mathcal{J}}_t$ we denote the Jacobian of the ALE map, $\widehat{\mathcal{J}}_t = \det \widehat{\nabla} \widehat{\mathcal{A}}_t$, where $\widehat{\nabla}$ is the gradient with respect to $\widehat{\mathbf{x}}$. In this context, we refer to $\widehat{\mathbf{x}} \in \widehat{\Omega}$ as the *ALE coordinate* while for $\mathbf{x} = \widehat{\mathcal{A}}_t(\widehat{\mathbf{x}}) \in \Omega(t)$ we refer to as an *Eulerian (or spatial) coordinate*. Let $f: \Omega(t) \times (0, T) \rightarrow \mathbb{R}$ and $\widehat{g}: \widehat{\Omega} \times (0, T) \rightarrow \mathbb{R}$ be two scalar fields defined on the current and the referential configurations, respectively. We define their *ALE* and *Eulerian* counterparts, respectively, by

$$\begin{aligned} \widehat{f}: \widehat{\Omega} \times (0, T) &\rightarrow \mathbb{R}, \widehat{f} = f \circ \widehat{\mathcal{A}}_t, \\ g: \Omega(t) \times (0, T) &\rightarrow \mathbb{R}, g = \widehat{g} \circ \widehat{\mathcal{A}}_t^{-1}. \end{aligned} \tag{22}$$

The time derivative of an Eulerian field f in the ALE frame – i.e. time derivative in the ALE frame, written with respect to the spatial coordinates – is defined as

$$\left. \frac{\partial}{\partial t} \right|_{\widehat{\mathbf{x}}} f: \Omega(t) \times (0, T) \rightarrow \mathbb{R}, \left. \frac{\partial}{\partial t} \right|_{\widehat{\mathbf{x}}} f(\mathbf{x}, t) = \frac{\partial \widehat{f}}{\partial t}(\widehat{\mathbf{x}}, t), \widehat{\mathbf{x}} = \widehat{\mathcal{A}}_t^{-1}(\mathbf{x}). \tag{23}$$

The time derivative of an Eulerian field in the spatial frame is just the classical time partial derivative

$$\left. \frac{\partial}{\partial t} \right|_{\mathbf{x}} f = \frac{\partial f}{\partial t}.$$

The domain velocity is defined by

$$\mathbf{w}(\mathbf{x}, t) = \left. \frac{\partial}{\partial t} \right|_{\widehat{\mathbf{x}}} \mathbf{x}, \mathbf{x} = \widehat{\mathcal{A}}(\widehat{\mathbf{x}}, t), \tag{24}$$

and the ALE temporal derivative by

$$\left. \frac{\partial}{\partial t} \right|_{\widehat{\mathbf{x}}} f = \frac{\partial f}{\partial t} + \mathbf{w} \cdot \nabla f. \tag{25}$$

As a result, by introducing an ALE temporal derivative instead of its Eulerian counterpart, an extra convective-type term, due to domain movement, will appear in the equation of interest.

In the ALE framework, the test function spaces are redefined by

$$\begin{aligned} \mathbf{V}_v &= \{\boldsymbol{\phi}: [0, T] \times \Omega \rightarrow \mathbb{R}^d \mid \boldsymbol{\phi}(\mathbf{x}, t) = \widehat{\boldsymbol{\phi}}(\widehat{\mathcal{A}}_t^{-1}(\mathbf{x})), \widehat{\boldsymbol{\phi}} \in \mathbf{H}_{n, \Gamma}^1(\widehat{\Omega})\}, \\ \mathbf{V}_p &= \{q: [0, T] \times \Omega \rightarrow \mathbb{R} \mid q(\mathbf{x}, t) = \widehat{q}(\widehat{\mathcal{A}}_t^{-1}(\mathbf{x})), \widehat{q} \in L_0^2(\widehat{\Omega})\}, \\ \mathbf{V}_c &= \{\psi: [0, T] \times \Omega \rightarrow \mathbb{R} \mid \psi(\mathbf{x}, t) = \widehat{\psi}(\widehat{\mathcal{A}}_t^{-1}(\mathbf{x})), \widehat{\psi} \in \mathbf{H}_{\Sigma}^1(\widehat{\Omega})\}, \\ \mathbf{V}_n &= \{\chi: [0, T] \times \Omega \rightarrow \mathbb{R} \mid \chi(\mathbf{x}, t) = \widehat{\chi}(\widehat{\mathcal{A}}_t^{-1}(\mathbf{x})), \widehat{\chi} \in \mathbf{H}^1(\widehat{\Omega})\} \end{aligned} \tag{26}$$

Hence, the test functions are time-independent in the reference frame, while they are time-dependent in the physical frame through the space variable \mathbf{x} . However, test functions are still time independent in sense of the material derivative, e.g.

$$0 = \frac{\partial \widehat{\psi}}{\partial t} = \left. \frac{\partial}{\partial t} \right|_{\widehat{\mathbf{x}}} \psi = \frac{\partial \psi}{\partial t} + \mathbf{w} \cdot \nabla \psi, \forall \psi \in \mathbf{V}_c(\Omega_t). \tag{27}$$

With all the necessary tools and function spaces introduced above, at this point we are able to derive the weak formulation of the CDC system in ALE framework. The problem in weak form reads: find (\mathbf{v}, p, c, n) such that

$c = 1$ on Σ and

$$\begin{aligned} \forall(\boldsymbol{\phi}, q, \psi, \chi) \in \mathbf{V}_v \times \mathbf{V}_p \times \mathbf{V}_c \times \mathbf{V}_n \\ \int_{\Omega} \left(\frac{\partial}{\partial t} \Big|_{\bar{\mathbf{x}}} \mathbf{v} \cdot \boldsymbol{\phi} + (\mathbf{v} - \mathbf{w}) \cdot \nabla \mathbf{v} \cdot \boldsymbol{\phi} + \text{Pr} \mathbb{D}(\mathbf{v}) : \nabla \boldsymbol{\phi} - \text{Pr} p \text{div} \boldsymbol{\phi} + \text{Ra Pr} n \mathbf{k} \cdot \boldsymbol{\phi} \right) dx \\ + \int_{\Gamma} \frac{1}{\beta_s} \mathbf{v} \cdot \boldsymbol{\phi} dS + \int_{\Sigma} \frac{\text{Pr}}{\text{Ca}} \nabla_{\Sigma} \text{id} : \nabla_{\Sigma} \boldsymbol{\phi} dS - \int_{\partial \Sigma} \frac{\text{Pr}}{\text{Ca}} \cos \theta_s \mathbf{t}_{\Gamma} \cdot \boldsymbol{\phi} ds = 0, \\ \int_{\Omega} \text{div} \mathbf{v} q dx = 0, \\ \int_{\Omega} \left(\frac{\partial}{\partial t} \Big|_{\bar{\mathbf{x}}} c \psi + (\mathbf{v} - \mathbf{w}) \cdot \nabla c \psi + \text{Le} \nabla c \cdot \nabla \psi + \text{Hr}(c) n \psi \right) dx = 0, \\ \int_{\Omega} \left(\frac{\partial}{\partial t} \Big|_{\bar{\mathbf{x}}} n \chi + (\mathbf{v} - \mathbf{w}) \cdot \nabla n \chi + \nabla n \cdot \nabla \chi - \text{Sr}(c) n \nabla c \cdot \nabla \chi \right) dx = 0. \end{aligned} \tag{28}$$

In the above weak formulations, \mathbf{w} is the domain velocity which has to satisfy a certain condition on the boundary $\partial \Omega$, more precisely

$$\mathbf{w} \cdot \mathbf{n} = \mathbf{v} \cdot \mathbf{n} \text{ on } \partial \Omega,$$

while it can be extended arbitrarily into the interior of the domain. We discuss later in more details a possible numerical realization of the domain (grid) velocity. All of the equations in system (28) are in non-conservative form. The conservative form of any of the equations can be obtained by, formally, extracting the temporal derivative in front of the integral sign and employing the *Reynolds transport theorem* in the process. Consequently, one extra term in the equation will appear in the form of domain velocity divergence. For illustration sake, consider the convection–diffusion equation for oxygen concentration. The transient term can be rewritten in the form of

$$\int_{\Omega} \frac{\partial}{\partial t} \Big|_{\bar{\mathbf{x}}} c \psi dx = \frac{d}{dt} \int_{\Omega} c \psi dx - \int_{\Omega} \text{div} \mathbf{w} c \psi,$$

where we underline the fact that test function ψ is time independent in the sense of material derivative. Although the formulations, conservative and non-conservative, are equivalent on the continuous level, on the discrete level one can be advantageous over the other depending on the problem of interest. For example, in conservative formulations an additional property, the so called *Space Conservation Law* (SCL), has to be satisfied by the numerical method while this issue does not appear in the nonconservative formulations. If the SCL is not satisfied, artificial sinks and sources may appear (see [14]). On the other side, conservative formulations have the advantage that the ALE term is itself in “conservative form” which might be desirable from the numerical point of view. For details on this manner and solutions to the problem we refer to [14,15,19,20]. In case of conservative formulation, we ensure that SCL is satisfied by employing the method developed and described in [20]. The mentioned approach (method developed in [20]) gives a systematic way of satisfying the discrete SCL independently on the chosen temporal discretization. Therefore, an easy adaptation to higher order temporal discretizations is possible which might be necessary in parametric studies. In this paper, however, all the numerical tests were performed employing the implicit Euler method for temporal discretization.

3.3. The numerical method

For solving the system (28) or its conservative variant, we employ the finite element method within Arbitrary Lagrangian–Eulerian framework. Passing from continuous to discrete level is a straightforward derivation from the weak form (28). Test function spaces are replaced by finite element spaces, thus enabling spatial discretization. This process is well known and for details we refer to, e.g., [7]. Temporal discretization is done by employing the finite difference type of schemes. In particular, in this paper all of the numerical results are obtained using the implicit Euler method.

In a discrete form, a function expressed through finite element basis functions is just an array of numbers corresponding to the nodes in the grid. However, since the nodes move in time, the same function is defined on different domains at different times. Thus, one has to pay an extra attention on the discretization involving

function at different time steps. In this paper a fully monolithic approach is employed. Essentially, it means that all equations are solved at once. This approach ensures a *strong coupling* between them (in contrast to *weak coupling* characteristic for partitioned approaches), although this increases the dimension of the discrete system to be solved. Note that all the unknowns at time $t \in (0, T)$ are defined on $\Omega(t)$ which is unknown itself at time t , and is an implicit function of the fluid velocity $\mathbf{v}(t) \cdot \mathbf{n}(t)$ on the boundary $\partial\Omega(t)$. This introduces an additional non-linearity in the system — these types of issues are characteristic for *fluid–structure interaction* (FSI) problems and in general for problems posed on time-dependent domains. We employ an iterative technique combined with Newton type linearization in order to find $\mathbf{n}^{n+1}, p^{n+1}, c^{n+1}, n^{n+1}$ at time t_{n+1} defined on Ω_{n+1} , provided that the previous step solution at time t_n is known. The algorithm is similar to that introduced in [21] for the FSI problems.

The ALE map describing the evolution of the domain is constructed via the grid velocity \mathbf{w} , whose calculation is decoupled from the chemotaxis system. Once the fluid velocity is known, the boundary velocity of the domain can be constructed. In order to obtain the grid velocity the harmonic extension technique is employed:

$$\begin{aligned} \Delta_n \mathbf{w}_{n,n+1} &= 0 \text{ in } \Omega_n \\ \mathbf{w}_{n,n+1} &= \boldsymbol{\omega}_{n,n+1} \text{ on } \partial\Omega_n, \end{aligned} \tag{29}$$

where $\mathbf{w}_{n,n+1}$ is the (constant in time) grid velocity on $(t_n, t_{n+1}]$ and $\boldsymbol{\omega}_{n,n+1}$ is the boundary velocity on $(t_n, t_{n+1}]$ constructed from the fluid velocity. Index n in differential operator denotes that it operates with respect to \mathbf{x}_n . The finite element space for grid velocity is piecewise linear, i.e. \mathbb{P}_1 , in order to preserve the straight edges of the mesh. Then, the ALE map is constructed as

$$\mathbf{x}_{n+1} = \mathbf{x}_n + \Delta t \mathbf{w}_{n,n+1} \tag{30}$$

where $\Delta t = t_{n+1} - t_n$. For alternative reconstruction of the domain velocity (e.g. continuous in time) and its connection to the SCL issues, we again refer to [20].

As already mentioned, the necessary condition for a volume to be preserved on a continuous level is that

$$\mathbf{w} \cdot \mathbf{n} = \mathbf{v} \cdot \mathbf{n} \text{ on } \partial\Omega, \tag{31}$$

i.e. the Dirichlet boundary conditions are given only in normal direction. Clearly, a trivial choice for the grid velocity on the boundary which satisfies this condition is $\mathbf{w} = \mathbf{v}$ on $\partial\Omega$. However, if tangential component of fluid velocity \mathbf{v} is large, this choice can result in an unnecessary large distortion and produce a bad quality mesh. From the viewpoint of physical interpretation of the problem, we can find a better candidate for grid boundary velocity. It is a physically reasonable assumption that no breaking of the waves will occur – i.e. bacteria will not influence the fluid strongly enough to produce breaking waves on the free surface. This is also an implicit assumption just by employing the ALE approach which cannot deal with the changes in the grid topology. Then, if there is no wave-breaking (waves can still travel in horizontal directions), the free surface is moving only in vertical direction $\mathbf{k} = [0, 1]^T$ in two dimensions and $\mathbf{k} = [0, 0, 1]^T$ in three dimensions. Then, the domain boundary velocity $\boldsymbol{\omega}$ can be defined as:

$$\boldsymbol{\omega} = \frac{\mathbf{v} \cdot \mathbf{n}}{\mathbf{k} \cdot \mathbf{n}} \mathbf{k} \text{ on } \partial\Omega \tag{32}$$

and the condition $\boldsymbol{\omega} \cdot \mathbf{n} = \mathbf{v} \cdot \mathbf{n}$ is satisfied. This condition, however, still does not guarantee that the volume will be preserved on discrete level. This is due to fact that incompressibility constraint is not preserved under the composition with ALE map, e.g. taking $\mathbf{v}_n \in H^1_{n,T}(\Omega_n)$ s.t. $\text{div}_n \mathbf{v}_n = 0$ in Ω_n does not imply that $\text{div}_{n+1}(\mathbf{v}_n \circ \mathcal{A}_n^{n+1}) = 0$. Here, \mathcal{A}_n^{n+1} denotes the mapping from Ω_n to Ω_{n+1} , $\mathcal{A}_n^{n+1} = \widehat{\mathcal{A}}_{n+1} \circ \widehat{\mathcal{A}}_n^{-1}$. This results in varying the total volume of the incompressible fluid inside the domain and, consequently, varying the total mass itself. Choosing sufficiently small time steps, this issue can be minimized, however, it will not vanish. In order to satisfy the total mass conservation, we incorporate an additional constraint into the calculation of the boundary grid velocity. We require that

$$\int_{\Omega_{n+1}} d\mathbf{x}_{n+1} = \int_{\Omega_n} d\mathbf{x}_n, \tag{33}$$

which can be rewritten in the form of

$$\int_{\Omega_n} (1 - \mathcal{J}_n^{n+1}) d\mathbf{x}_n = 0, \mathcal{J}_n^{n+1} = \det \nabla_n \mathcal{A}_n^{n+1}. \tag{34}$$

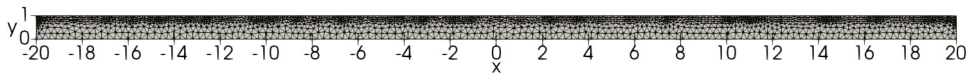


Fig. 4. Initial mesh in the two dimensional case. *FreeFem++* offers `adaptmesh` operator which can locally refine the mesh given the desired metrics.

This is an isoperimetric constraint that can be handled by means of Lagrangian multiplier within the classical techniques of *calculus of variations*. In this case (an isoperimetric constraint variational approach), the Lagrangian multiplier λ is just a real number, thus increasing the system to be solved from order n to $n + 1$ although introducing an additional nonlinearity in the system through the nonlinear constraint.

4. Numerical simulations: influence of the dynamic free surface

In this section we provide some chosen results of the numerical simulations and emphasize the influence of the dynamic free surface. Simulations are performed in both two and three dimensions and with both fixed and dynamic free surfaces. All simulations are done in *FreeFem++* software (see [22,23]) while the visualization is displayed by *Paraview* (see [24]).

The (dimensionless) computational domain is chosen such that it corresponds to the *Petri dish* (a shallow cylinder in 3d or rectangle in 2d) with diameter of 10 cm and height of 2.5 mm – a common setup in the laboratory experiments. The domain is triangularized into the finite number of triangles (in 2d) and tetrahedra (in 3d) resulting in the computational mesh. In order to capture the singularities near the contact points (line) and the behavior near free surface, mesh is refined in these areas (see Fig. 4 and also Fig. 8).

In 2d case, Lagrangian finite element spaces of order two and one respectively are chosen for velocity and pressure of the fluid, $(\mathbf{v}_h, p_h) \in [\mathbb{P}_2]^2 \times \mathbb{P}_1$. This combination of spaces is known to satisfy the *Ladyženskaya–Babuška–Brezzi* (LBB) condition. The spaces for concentrations c_h and n_h are both Lagrangian finite element spaces of order two, \mathbb{P}_2 .

In 3d case, Lagrangian finite element spaces of order one enriched with bubble element are chosen for velocity and Lagrangian finite element spaces of order one for pressure, $(\mathbf{v}_h, p_h) \in [\mathbb{P}_{1b}]^3 \times \mathbb{P}_1$. This combination of spaces is known to satisfy the (LBB) condition. The spaces for concentrations c_h and n_h are both Lagrangian finite element spaces of order one, \mathbb{P}_1 . The lower orders of finite element spaces in 3d are chosen in order to reduce the dimension of the system which is significantly larger than that in 2d case. Putting aside the computational time to run the simulation, for dense grids it is even possible that the system does not fit in the memory. Rather than using the partitioned approach, we decided to reduce the order of the elements. However, in the future we attempt to parallelize the algorithm in 3d in order to make the calculations with higher order elements possible.

Most of the implementation within the *FreeFem++* environment is fairly standard and is a straightforward projection of the model into the finite element language. The problematic and “non-traditional” part is the implementation of the boundary conditions on the contact line (points), which has to be done “by hand” (traditionally, the boundary conditions are posed only on $(d - 1)$ -dimensional boundaries). Degrees of freedom that correspond to the contact points (line) for chosen function spaces have to be extracted in order for the integration on $\partial\Omega$ to be performed. Below, we give an easy way to extract such $(d - 2)$ -dimensional boundaries.

```

1 // extracting dofs on contact points for [P2,P2,P1,P2,P2] in case of two
   // dimensional domain
2
3 mesh th0; // initial mesh
4
5 // boundary labels
6 int bottom=1,
7     freeSurf=2,
8     wx0=3, wx1=4;
9 int[int] walls = [wx0,wx1];
10
11 // number of dofs on contact points for [P2,P2,P1,P2,P2]
12 int nOfCpDofs=4;

```

```

13 int[int] DofsOnCp(nOfCpDofs);
14 {
15     fespace Vh(th0, [P2, P2, P1, P2, P2]);
16
17     varf vf1([u1, u2, u3, u4, u5], [v1, v2, v3, v4, v5]) = on(walls, u1=1, u2=1);
18     varf vf2([u1, u2, u3, u4, u5], [v1, v2, v3, v4, v5]) = on(freeSurf, u1=1, u2=1);
19
20     real[int] dofsOnWalls = vf1(0, Vh, tgv=1);
21     real[int] dofsOnSurf = vf2(0, Vh, tgv=1);
22
23     int counter=0;
24     for(int k=0; k<Vh.ndof; ++k) if(dofsOnWalls[k]==1 && dofsOnSurf[k]==1) {
25         DofsOnCp[counter]=k;
26         ++counter;
27     }
28 }

```

```

1 // extracting dofs on contact line for [P1b, P1b, P1b, P1, P1, P1] in case of three
2 // dimensional domain
3 mesh3 th0;
4
5 // boundary labels
6 int bottom=1,
7     freeSurf=2,
8     wy0=3, wx1=4, wy1=5, wx0=6;
9 int[int] walls = [wy0, wx1, wy1, wx0];
10
11
12 func int[int] IsolateDofsOnContactLine(mesh3& th, int[int] walls, int freeSurf){
13
14     fespace Vh(th, [P1b, P1b, P1b, P1, P1, P1]);
15
16     varf v1([u1, u2, u3, p, c, n], [v1, v2, v3, q, r, s]) = on(walls, u1=1, u2=1, u3=1);
17     varf v2([u1, u2, u3, p, c, n], [v1, v2, v3, q, r, s]) = on(freeSurf, u1=1, u2=1, u3=1);
18
19     real[int] dofsOnWalls = v1(0, Vh, tgv=1);
20     real[int] dofsOnSurf = v2(0, Vh, tgv=1);
21
22     int nOfClDofs=0;
23     for(int k=0; k<Vh.ndof; ++k) if(dofsOnWalls[k]==1 && dofsOnSurf[k]==1) ++
24         nOfClDofs;
25
26     int[int] dofsOnCl(nOfClDofs);
27
28     int counter=0;
29     for(int k=0; k<Vh.ndof; ++k) if(dofsOnWalls[k]==1 && dofsOnSurf[k]==1) {
30         dofsOnCl[counter]=k;
31         ++counter;
32     }
33
34     return dofsOnCl;
35 };
36
37 int[int] dofsOnCl = IsolateDofsOnContactLine(th0, walls, freeSurf);
38 int nOfDofsOnCl = dofsOnCl.n; // number of dofs on contact line

```

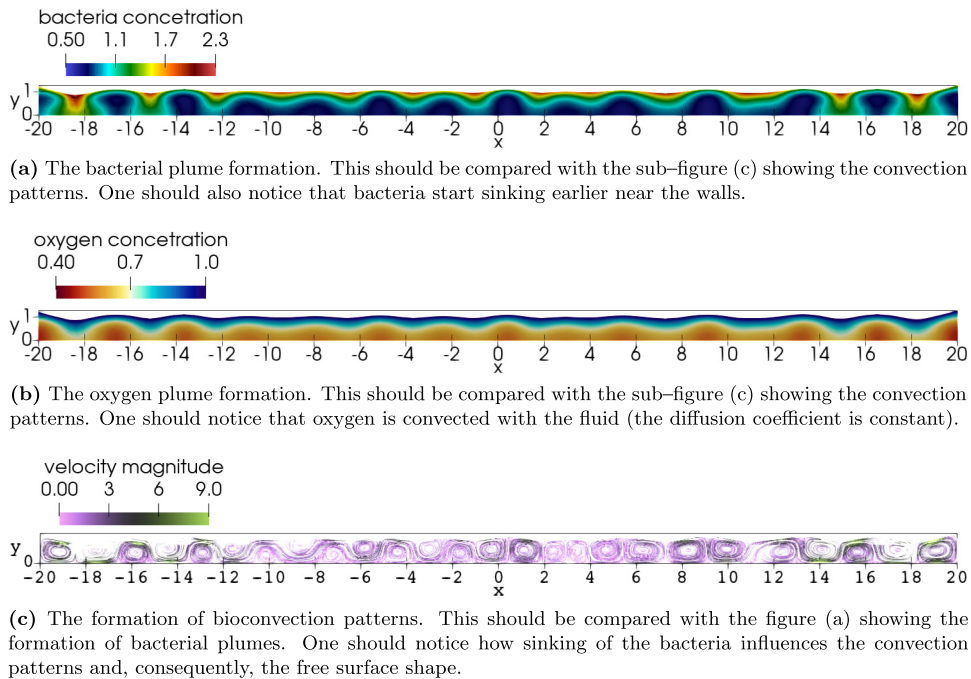


Fig. 5. The chemotaxis phenomenon state at time $t = 1.9$ in 2D case.

This procedure is necessary only when the mesh and finite element spaces on it are firstly constructed (and, eventually, if at some point in the algorithm the mesh and the finite element spaces are reconstructed). This is due to the fact that `movemesh` operator does not change the labels or the numbering of vertices of the mesh (and, consequently, the numbering of the degrees of freedom). After the contact points (line) are identified, the last term in (28) can be evaluated (integral over $\partial\Sigma$) and added to the right hand side vector of the linear system.

4.1. Numerical results

Below, the results illustrating the chemotaxis phenomenon are presented. The case corresponds to the following selection of the dimensionless numbers: $Pr = 7700$, $Ra = 400$, $S = 2$, $H = 1$, $Le = 1$, $Ca = 10^{-2}$, $\beta_s = 10^{-3}$, $Fr = 10^{-3}$, $\theta_s = 3\pi/8$ (where the last four parameters appear do not appear in the fixed free surface case). The surface tension is taken to be constant independently of bacteria concentration ($\sigma = \sigma_0$).

Apart from the different plume shapes and bioconvection patterns, which are an expected difference, the major effect of the free surface is the time scale at which sinking of the bacteria occurs. In the case where free surface is allowed to deform, the instabilities due to density difference occur earlier causing the bacteria to sink to the bottom. This is most likely due to the fluid momentum built at the free surface which causes the enlargement of convection terms in magnitude. Convection works unfavorably towards the bacteria tendency to stay at the oxygen-rich free surface. Together with gravity effects, it causes the bacteria to fall at the bottom. During the sinking, bacteria greatly influence the convection of fluid and the formation of convection patterns (see Fig. 5). Eventually, the stationary solution is reached where bacteria are “trapped” in the fluid vortex (see Figs. 6 and 7). The migration of the bacteria is dominated by the fluid convection patterns rather than its directional swimming (which is too weak in comparison with the fluid convection). Both oxygen and bacteria are convected with the fluid. The free surface shape is determined by convection patterns balanced with the static angle on the contact line.

In Fig. 5 it is demonstrated how the bioconvection patterns are formed under the influence of sinking of the bacteria. The figure shows the state of the phenomenon when the density gradient of the suspension grows large enough to cause the sinking of the bacteria densely packed in a thin layer below the free surface.

In the present case, sinking firstly occurs near the walls due to capillary effects and (relatively) large static contact angle. The contact line is slightly above the free surface so the bacteria pack slightly denser in the immediate

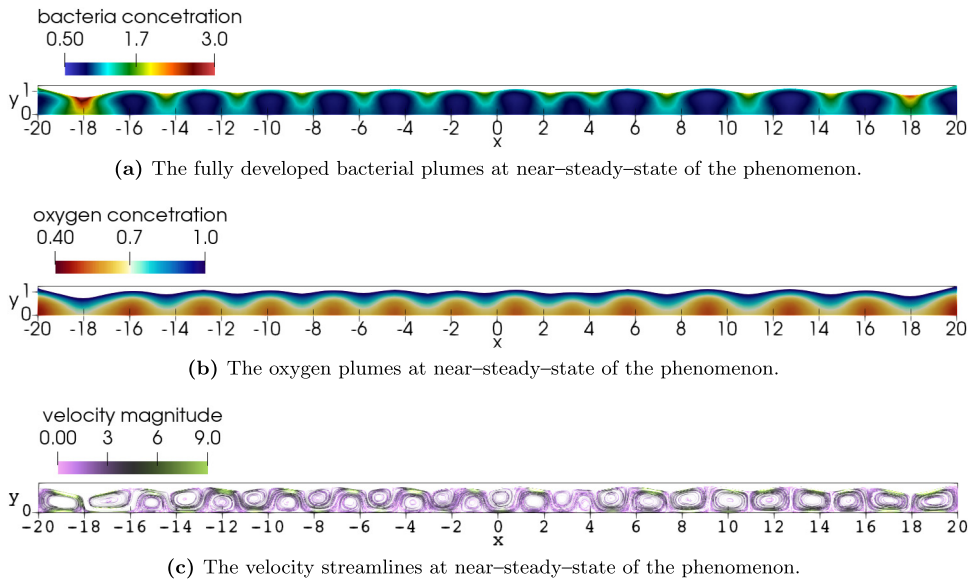


Fig. 6. The chemotaxis phenomenon state at time $t = 2.6$ in 2D case.

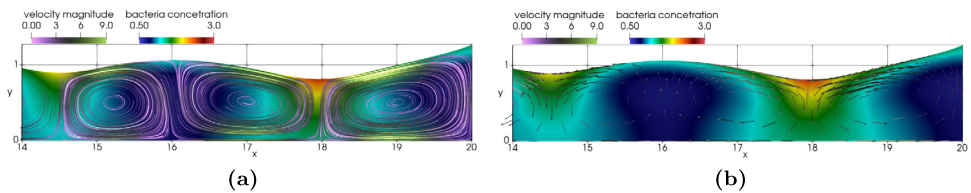


Fig. 7. The bacteria concentration and convection patterns (the velocity streamlines in (a) and the velocity glyphs in (b)) near the right wall in 2D case. The figure demonstrates how the bacteria are trapped in the fluid vortex at near-steady-state time of the phenomenon.

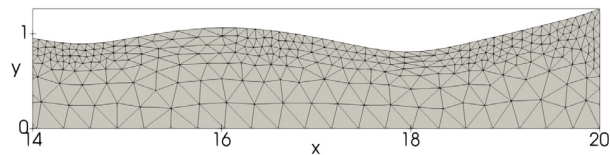


Fig. 8. Magnified 2D domain in the contact point neighborhood at the time when stationary solution is almost reached.

neighborhood of the wall than on the rest of the free surface due to the gravity pull. Thus, the plume formation is greatly influenced by the boundary conditions. The influence of boundary conditions is very clearly seen in the 3D case observing the fluid velocity streamline patterns near the wall (compare with Fig. 11(b)). The contact angle and the friction-slip coefficient seem to play the central role here, however, this outreaches the scope of this paper and it might be considered in one of the following parametric studies.

In Fig. 8, the domain magnified in the contact point neighborhood is shown at the time when stationary solution is almost reached. The balance between forces produced by the capillary effect and the static contact angle, and the forces resulting from the convection patterns, is soon to be reached.

In the three dimensional case, the global behavior of the phenomenon follows the same trend as in two dimensional case. In Figs. 9 and 10 bacteria concentration and velocity patterns are shown at the time when bacteria start sinking and bacterial plumes start forming. Although calculations are performed on relatively coarse mesh and with lower order finite elements, simulation results show good agreement with what can be expected from the two dimensional case. One can notice that by extracting slices of the three dimensional domain, bioconvection patterns and bacteria concentration follow a very similar trend as in the two dimensional case (compare Figs. 5 and 9).

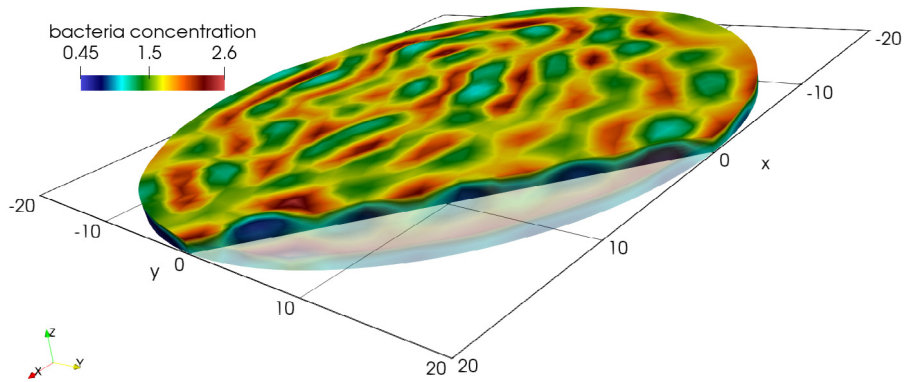
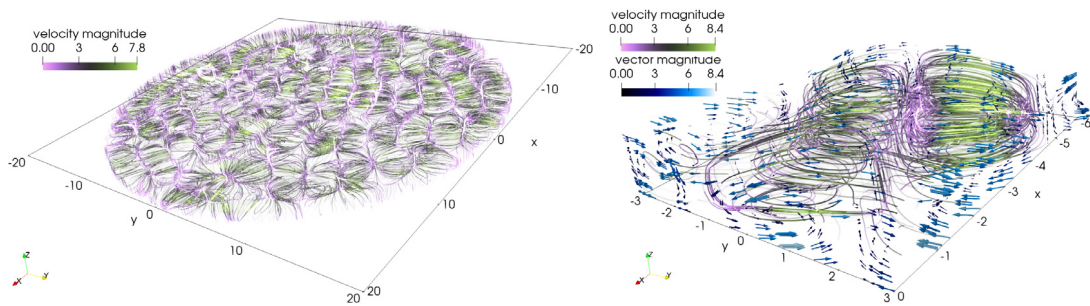


Fig. 9. The formation of the bacterial plumes (at time $t = 2.6$). The domain is *clipped* in order to illustrate the plume formation inside the domain — on the cross section.



(a) Velocity streamlines. This Figure should be compared with Figure 9. (b) Magnified clip of the fluid convection patterns from the figure (a) together with vector glyphs.

Fig. 10. Velocity streamlines and glyphs corresponding to bacterial plume formations given on Fig. 9.

Fig. 11 shows the bacteria concentration and velocity streamlines from the top. If one compares these results with Figure 1 in [2], which shows the photograph of the bioconvection patterns that form in a circular Petri dish from a real experiment, unquestionable similarities can be seen. Our simulated patterns follow very similar trends to those obtained experimentally in [2], although, the physical parameters of the system are not exactly the same. We believe that increasing the mesh density would even further improve the numerical results, thus enabling the proposed model to simulate the chemotaxis phenomenon very credibly. We refer the reader to pay particular attention to Fig. 11 (b) which shows the velocity streamlines patterns. The formation of regular convection patterns (square, pentagonal and hexagonal) characteristic for the *Bénard* convection can be observed.

5. Conclusion

A new model for chemotaxis–diffusion–convection coupling system has been derived and a numerical method for simulating the accompanied phenomena has been proposed in two and three dimensions. The novelty is in considering the influence of bioconvection on the motion of the free surface and *vice versa*. The influence of moving free surface on the overall phenomenon is also addressed. Both surface tension phenomenon and dynamic contact line have been considered and incorporated into the model restricting the simplifications to a minimum level. Boundary conditions for incorporating these two issues have been proven to be quite problematic from the numerical point of view in continuum mechanics approach, however, very realistic results have been obtained using the approach described in this paper. The non-dimensionalization of the upgraded model has been proposed in parallel to already existing non-dimensionalization by adding some extra dimensionless parameters due to the introduction of new terms in the governing equations.

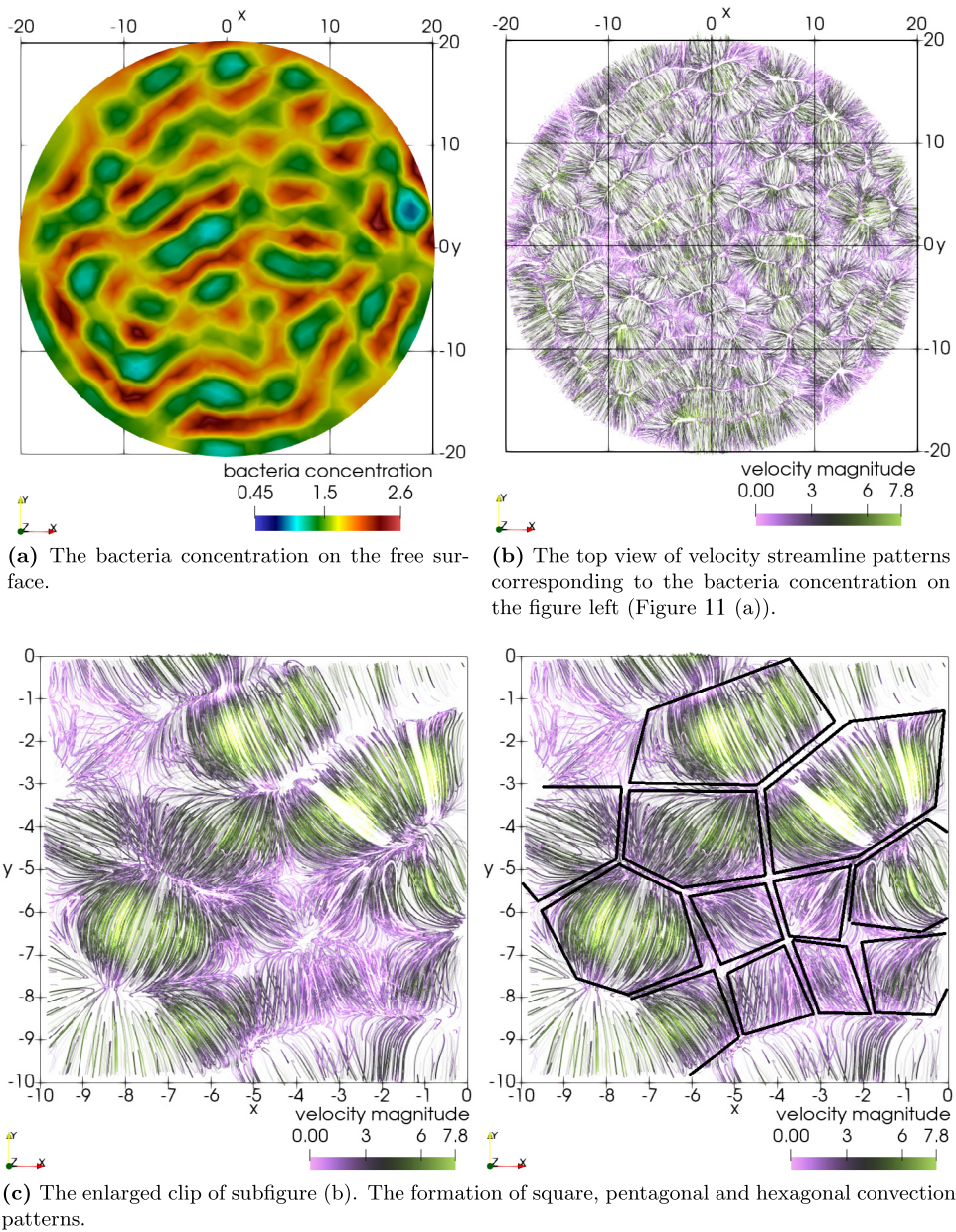


Fig. 11. The top view of the state of the phenomenon at time $t = 2.6$.

The numerical studies showed the significant influence of dynamic free surface on the chemotaxis process. Apart from the noticeable change in bioconvection patterns in comparison with the patterns obtained for the same physical parameters but with fixed surface, the main difference seems to be in a resulting time scale. Keeping the surface fixed allows bacteria to pack denser in a thin layer below the surface as well as makes it easier for them to stay near the surface for longer time in comparison with the dynamic surface case. In the dynamic surface case the momentum due to difference in the suspension density is built easier which makes it harder for bacteria to stay on the free surface. This might play a significant role in real applications since time scale on which process is taking place is an important consideration. Also, it opens a new insight on the non-linear dynamics of phenomenon. In 3D case, the numerical results in the present paper have shown very good agreement with experimental observation and the intuition despite the fact that the calculations have been performed on (relatively) coarse mesh.

In the following papers a detailed parametric study will be performed in both two and three dimensions. For a three-dimensional case a parallelization of the numerical method might be necessary since an enlargement of the system is significant in comparison with the two-dimensional case.

Acknowledgments

This work was supported in part by NHRI (National Health Research Institutes, Institute of Biomedical Engineering and Nanomedicine, Zhunan, Taiwan, project number BN-106-PP-08) and MOST (Ministry of Science and Technology, Taipei, Taiwan, project number MOST-106-2115-M-400-001-) project.

References

- [1] J.O. Kessler, Path and pattern – the mutual dynamics of swimming cells and their environment, *Comm. Theoret. Biol.* 1 (1989) 85–108.
- [2] A.J. Hillesdon, T.J. Pedley, J.O. Kessler, The development of concentration in a suspension of chemotactic bacteria, *Bull. Math. Biol.* 57 (2) (1995) 299–344.
- [3] A.J. Hillesdon, T.J. Pedley, Bioconvection in suspensions of oxytactic bacteria: linear theory, *J. Fluid Mech.* 324 (1996) 223–259.
- [4] A. Chertock, K. Fellner, A. Kurganov, A. Lorz, P.A. Markowich, Sinking, merging and stationary plumes in a coupled chemotaxis–fluid model: a high resolution numerical approach, *J. Fluid Mech.* 694 (2012) 155–190.
- [5] Y. Deleuze, C.-Y. Chiang, M. Thiriet, T.W.-H. Sheu, Numerical study of plume patterns in a chemotaxis–diffusion–convection coupling system, *Comput. Fluids* 126 (2016) 58–70.
- [6] S. Chakraborty, F. Ivancic, M. Solovchuk, T.W.-H. Sheu, Stability and dynamics of a chemotaxis–diffusion–convection system in a shallow fluid layer, *Phys. Fluids* 30 (2018) 071904.
- [7] P.G. Ciarlet, *The Finite Element Method for Elliptic Problems*, North-Holland, Amsterdam, New York, Oxford, 1978.
- [8] A. Quarteroni, A. Valli, *Numerical Approximation of Partial Differential Equations*, Springer-Verlag, Berlin, Heidelberg, 1994.
- [9] J. Donea, A. Huerta, J.-Ph. Ponthot, A. Rodríguez-Ferran, Arbitrary Lagrangian–Eulerian methods, *Ency. Comput. Mech.* 1 (2004) 413–437 (Chapter 14).
- [10] T.Z. Qian, X.P. Wang, P. Sheng, Molecular scale contact line hydrodynamics of immiscible flows, *Phys. Rev. E* 68 (2003) 016306.
- [11] T.Z. Qian, X.P. Wang, P. Sheng, Molecular scale contact line in two–phase immiscible flows, *Commun. Comput. Phys.* 1 (2006) 1–52.
- [12] S. Ganesan, L. Tobiska, Modelling and simulation of moving contact line problems with wetting effects, *Comput. Vis. Sci.* 12 (2009) 329–336.
- [13] J.-F. Gerbeau, T. Lelièvre, Generalized Navier boundary condition and geometric conservation law for surface tension, *Comput. Methods Appl. Mech. Engrg.* 198 (2009) 644–656.
- [14] P.D. Thomas, C.K. Lombard, The geometric conservation law and its applications to flow computations on moving grids, *AIAA J.* 17 (1979) 1030–1037.
- [15] L. Formaggia, F. Nobile, A stability analysis for the arbitrary Lagrangian Eulerian formulation with finite elements, *East-West J. Num. Math.* 7 (1999) 105–132.
- [16] K.A. Cliffe, S.J. Tavener, Marangoni–Bénard convection with a deformable free surface, *Comput. Phys.* 145 (1998) 193–227.
- [17] F. Roohbakhshan, R.A. Sauer, A finite membrane element formulation for surfactants, *Colloids Surf. A* 566 (2019) 84–103.
- [18] M.C. Ruzicka, On dimensionless numbers, *Chem. Eng. Res. Des.* 86 (2008) 835–868.
- [19] C. Klingenberg, G. Schnücke, Y. Xia, An arbitrary Lagrangian–Eulerian local discontinuous Galerkin method for Hamilton–Jacobi equations, *J. Sci. Comput.* 73 (2017) 906–942.
- [20] F. Ivančić, T.W.-H. Sheu, Maxim Solovchuk, ALE–Type FEM formulation for PDEs on time–dependent domains with vanishing discrete SCL, *SIAM J. Sci. Comput.* 41–3 (2019) A1548–A1573.
- [21] O. Pironneau, An energy preserving monolithic eulerian fluid–structure numerical scheme, 2016, hal–01348648v1.
- [22] F. Hecht, New development in freefem++, *J. Numer. Math.* 20 (3–4) (2012) 251–265.
- [23] A. Decoene, B. Maury, Moving meshes with FreeFem++, *J. Numer. Math.* 20 (3–4) (2012) 195–214.
- [24] J. Ahrens, B. Geveci, C. Law, *ParaView: An End-User Tool for Large Data Visualization*, *Visualization Handbook*, Elsevier, 2005, ISBN-13: 978-0123875822.